Loop-mirror-based slot waveguide refractive index sensor

Jun-long Kou, Fei Xu, and Yan-qing Lu

Citation: AIP Advances **2**, 042142 (2012); doi: 10.1063/1.4768266
View online: http://dx.doi.org/10.1063/1.4768266
View Table of Contents: http://aipadvances.aip.org/resource/1/AAIDBI/v2/i4
Published by the American Institute of Physics.

Loop-mirror-based slot waveguide refractive index sensor

Jun-long Kou, Fei Xu,[a] and Yan-qing Lu[b]
National Laboratory of Solid State Microstructures and College of Engineering and Applied Sciences, Nanjing University, Nanjing 210093, P. R. China

(Received 16 August 2012; accepted 6 November 2012; published online 12 November 2012)

Loop mirror has been widely used in fiber optical devices and systems for it provides a smart way to make use of the fiber birefringence properties and can enhance the sensitivity greatly. On the other hand, slot waveguide is very promising for optical sensing applications because of their peculiar spatial mode profile. In this paper, we propose and analyze a loop-mirror-based slot waveguide (LMSW) sensor which can be routinely fabricated in modern high-volume complementary metal-oxide–semiconductor (CMOS) process. The finite element method (FEM) simulation results show that the birefringence can be as high as 0.8 which is orders of magnitude than that in conventional birefringent fiber loop mirror. High sensitivity up to 6×10^3 nm/RIU (refractive index unit) is achieved by this scheme. [http://dx.doi.org/10.1063/1.4768266]

I. INTRODUCTION

Due to the progress of silicon processing technology which enables millimeter-scale devices with nanometer precision and being transparent at infrared telecom wavelengths, silicon-on-insulator (SOI) is suitable for use in passive linear devices and is likely to become the mainstay of the photonics industry. Over the past years, an impressive range of SOI devices, including splitters, filters, modulators and sensors, has been realized based on different kind of waveguides, among which there exists one that guides and confines light in a low-index region,[1,2] the slot waveguide. In addition, attributed to its interesting intrinsic properties, slot waveguide has also been extended to other material systems, e.g., silica fibers,[3,4] silicon nitride / silicon oxide platform,[5] *et al.*

The unique structure of the slot waveguide enhances the optical field confinement in low index materials and has inspired innovations including all-optical high-speed signal processing by employing silicon-organic hybrid slot waveguides combining polymer possessing a fast electronic third-order nonlinearity,[6] optical manipulation of nanoparticles and biomolecules in sub-wavelength slot waveguides,[7] slot waveguide based splitters for broadband terahertz radiation,[8] low-loss compact-size slot waveguide polarization rotator and transformer,[9] slot waveguide biochemical sensor,[10–14] *et al.* In particular, the sandwiched photonic structure permits a stronger light-analyte interaction as compared to that achievable by a conventional waveguide. As a result, the reported slot-waveguide sensor exhibited refractive index sensitivity as high as several hundreds of nm/RIU (refractive index unit). Moreover, considering the contrast field distribution between orthogonal modes, slot waveguide can possess high birefringence. This has enabled applications in fields such as delay lines,[15] broadband and highly efficient second harmonic generation in double-slot lithium niobate waveguides through phase matching,[16] *et al.* To our knowledge, however, all the previous slot waveguide sensors are based on ring resonators, Mach-Zenhder interferometers, directional couplers or Fabry-Perot cavities without employing the outstanding birefringence properties.[11]

On the other hand, highly birefringent fiber based loop mirror has been attractive as an element in optical fiber communications and optical fiber sensing,[17] e.g., in wavelength division multiplexing

[a]feixu@nju.edu.cn
[b]yqlu@nju.edu.cn

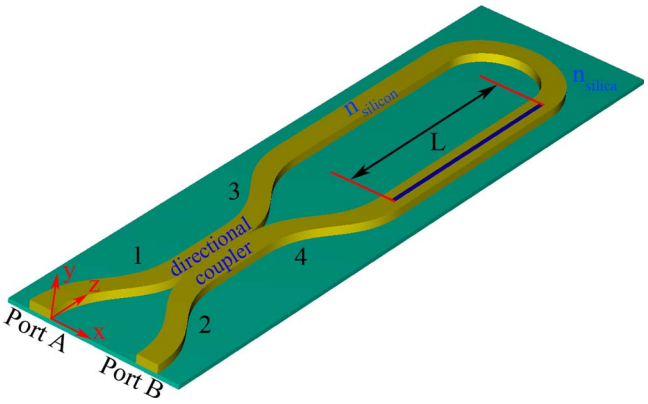

FIG. 1. Schematic of the loop-mirror-based slot waveguide sensor. The light is launched in through Port A in z-direction and received at Port B. The green, yellow and blue part is the substrate, silicon waveguide and slot, respectively. Other parameters are labeled in the picture.

filters, in gain flattening of Erbium-doped fiber amplifiers, in multi-wavelength fiber lasers and in dispersion tailoring, in optical gyroscope, in strain and temperature measurement, in liquid level and displacement sensing as well as a spectral filter for fiber Bragg grating demodulation.

In this article, we combine slot waveguide with loop mirror to devise a compact loop-mirror-based slot waveguide (LMSW) scheme and analyze its refractive index sensing properties by assuming the loop is immersed in ambient medium, e.g., air and water with the aid of finite element method (FEM) simulation. When compared with conventional sensors merely exploiting the evanescent field, sensitivity has been enhanced by several times to orders of magnitudes. The high sensitivity and compact size presents the LMSW great potentials to be integrated with other COMS-compatible photonic elements.

II. LMSW SENSOR: SIMULATION MODEL

Figure 1 is the schematic of the proposed LMSW sensor. It consists of a loop of silicon waveguide, including the slot region, formed between the output ports (Leg 3 and 4) of a directional coupler. In practice, it is convenient to fabricate such a scheme by standard deep-UV lithography or focused ion beam method. Broadband light is launched into Leg 1 via Port A, part of the light travels toward Leg 3 while the rest is coupled to Leg 4 of the loop, given that no loss occurs in the coupling region. Assuming that the coupler is a 50/50 one, therefore half of the input light travels clockwise around the loop while the other half travels counterclockwise. Light with different wavelength experiences different phase delay and polarization rotation after passing through the highly birefringent slot region. When light is finally collected at Port B by an optical spectrum analyzer, there appear interference patterns which are used for data interpretation. If the refractive index of the medium (i.e. air or water considered here) that covers the slot region changes, the birefringence varies accordingly which will finally be reflected in the shift of the interference patterns. Though light also experience birefringence outside the slot region, the birefringence is one order of magnitude less than that of the slot region. Hence, the birefringence outside the slot region is not considered here in order to give a more clear investigation into the main idea of the article. In addition, the modification of external environment can influence the coupling coefficient of the coupler,[18,19] that is the relative portion of light entering in Leg 3 and 4 and thus only influence the visibility of the polarimetric interference. As a result, here, we neglect the influence of the external environment on the directional coupler and only consider the effect in the slot region. Moreover, the directional coupler could be totally isolated from the external environment by adding an additional covering layer such as silica or low index polymer.

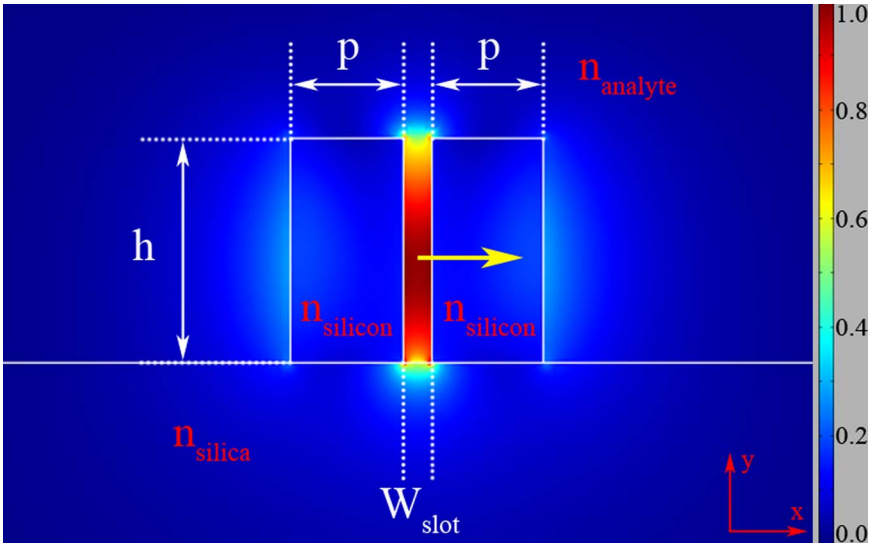

FIG. 2. Cross sectional electric field distribution of the slot waveguide with the fundamental quasi-TE mode. $n_{analyte}$, $n_{silicon}$ and n_{silica} denotes the refractive index of the immediate medium to be sensed, silicon and silica substrate with white solid line indicating the boundary of different materials. h, p and W_{slot} is the height, width of the silicon rib and width of the slot, respectively. The mode field is calculated at p = 200 nm, h = 400 nm and W_{slot} = 50 nm with the yellow arrow denoting the polarization direction.

III. RESULTS AND DISCUSSION

A. High Birefringence of the Slot Waveguide

Cross section of the slot waveguide is shown in Fig. 2 with all parameters concerning the geometry and refractive index explicitly labeled in the picture. We only consider the fundamental quasi-TE and quasi-TM mode that are orthogonally polarized. These two modes are true guided modes and there are no confinement losses. The non-degeneracy of the modes is known as phase birefringence B of the slot waveguide, and is defined as: $B = n_{eff}^{TM} - n_{eff}^{TE}$, where n_{eff}^{TE} and n_{eff}^{TM} are effective refractive indices of the quasi-TE and quasi-TM modes, respectively. As can be deduced from Fig. 2, in order to satisfy the continuity of the normal component of electric flux density D (i.e. $D_{1n} = D_{2n}$), the corresponding electric field (E-field) must experience a large discontinuity with much higher amplitude in the slot side (the low index analyte) in the case of quasi-TE mode (x-polarized). Due to the high-index-contrast interface of silicon and analyte, much field power will be strongly confined in the slot region, resulting in a much lower effective refractive index. Whereas in the case of quasi-TM mode (y-polarized), $D_{1n} = D_{2n}$ is naturally satisfied and light is mostly confined in the high index silicon, leading into a relatively higher effective refractive index.

Birefringence at 1550 nm is calculated assuming that the slot region is immersed in different analytes ($n_{analyte}$ ranging from 1.00 to 1.35, which is typically used for characterizing sensors) and the results are shown in Fig. 3. As Fig. 3(a) and 3(b) shows, high birefringence up to 0.3–0.8 (in air) and 0.1–0.6 (in water) can be achieved, which is one to two orders of magnitude higher than in conventional polarization maintaining fibers or highly birefringent microfibers. In addition, the birefringence first goes up quickly and then drops slowly as an increase of slot width (W_{slot}) given that h is smaller than 350 nm which is the typical thickness of a silicon-on-insulator wafer. The relatively flat behavior of the curve in the W_{slot} range 50–160 nm relieves the waveguide from fabrication precision. Moreover, a larger value of h results in a higher B. Nevertheless, that imposes a strict requirement on W_{slot} in order to guarantee the desired fundamental modes. From Fig. 3(c), we learn that B drops as $n_{analyte}$ increases because under this condition, the extent of refractive index asymmetry is lowered. One more point to notice is that at bigger h and larger W_{slot}, the two ribs made of silicon tends to support light field confined in the ribs independently and the modes in the two silicon ribs become decoupled, being unable to form the mode which concentrates the field in

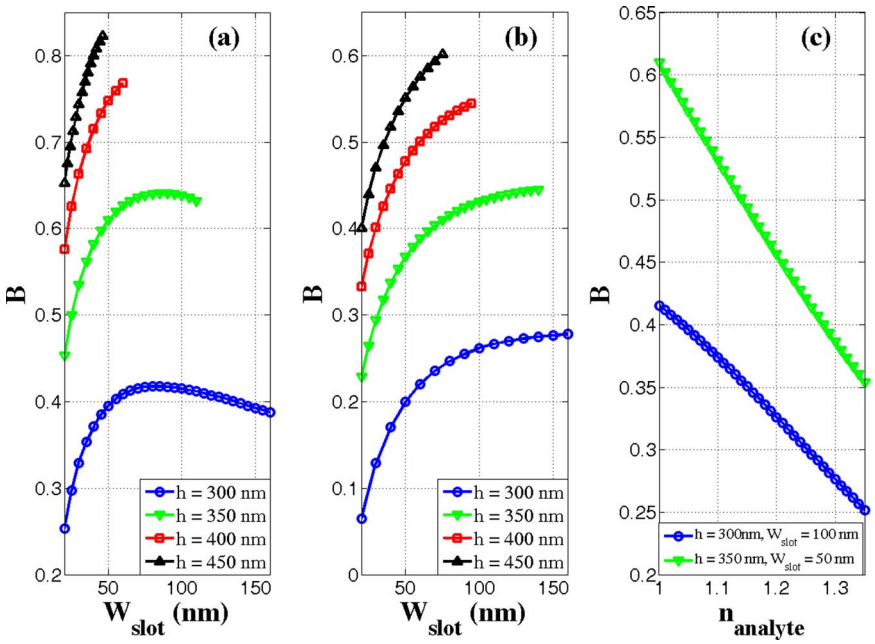

FIG. 3. Birefringence of the slot waveguide as a function of the width of the slot with analyte chosen to be (a) air and (b) water. (c) Birefringence of the slot waveguide as a function of $n_{analyte}$ for two fixed geometric configurations. Lines of different colors represent slot waveguide with different geometric parameters as indicated in Fig. 2. All calculations are performed at p = 200 nm and telecom wavelength 1550 nm.

the slot region as illustrated in Fig. 2 above. Concerning this, we do not include those simulation results in the article.

B. Refractive Index Sensitivity of LMSW

The transmission spectrum of the LMSW can be calculated via[17]

$$T(\lambda) \propto \left[\cos\left(\frac{\pi BL}{\lambda}\right)\right]^2 \tag{1}$$

where L is the length of the slot region and λ is the operating wavelength. Due to the high birefringence of the slot waveguide ($\sim 10^{-1}$ shown in Fig. 3) and considering the operating range of common light sources found in labs, the length of the slot region up to hundreds of micrometers is enough to get a reasonable free spectral range according to Eq. (1). Let us assume B, L and λ is 0.4, 200μm and 1550 nm, respectively. The free spectral range (FSR, λ^2/BL) turns out to be 30 nm. The variation of refractive index of external analyte causes changes of the birefringence of the slot region and thus the final interference patterns received at Port B. The shift of the interference wavelength λ_0 with respect to the analyte index change lays the foundation of the sensing principle. Sensitivity of the analyte ($S_{analyte}$) exploiting birefringence is defined in Eq. (2)[4] and the results are shown in Fig. 4(a) and 4(b). As can be deduced, sensitivity as high as 1×10^3 to 4×10^3 nm/RIU can be easily achieved over a wide range of geometrical parameters. Although sensitivity tends to decrease as an increase of W_{slot}, it still maintains in a high level ($>10^3$ nm/RIU). Moreover, $S_{analyte}$ reaches at very high value for $W_{slot} < 40$ nm. Thus, controlling the width of the slot is a key point in achieving a very high sensitivity.

$$S_{analyte} = \frac{\partial \lambda_0}{\partial n_{analyte}} = \frac{\partial \lambda_0}{\partial B}\frac{\partial B}{\partial n_{analyte}} = \frac{\lambda_0}{B}\frac{\partial B}{\partial n_{analyte}}. \tag{2}$$

Calculation is also performed in order to compare the results with sensitivity of the scheme that merely utilizes the principle of evanescent field of each mode (sensitivity is defined in Eq. (3))

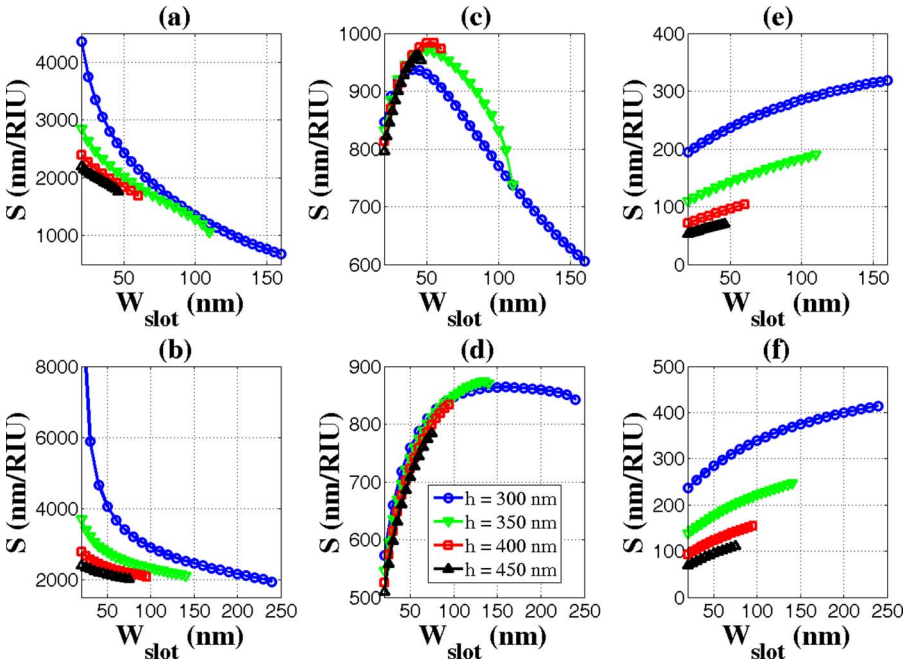

FIG. 4. $S_{analyte}$ exploiting the principle of birefringence as a function of W_{slot} when the LMSW is immersed in different ambient analyte, (a) for air and (b) for water. Sensitivity exploiting the principle of evanescent field as a function of W_{slot} when the LMSW is immersed in different ambient analyte, (c) and (e) for air, (d) and (f) for water. (c) and (d) represent quasi-TE mode while (e) and (f) represent quasi-TM mode. The blue, green, red and black lines are plotted when h equals 300 nm, 350 nm, 400 nm and 450 nm, respectively. All calculations are performed at p = 200 nm and telecom wavelength 1550 nm.

but not the birefringence. The results are presented in Fig. 4(c)–4(f) and are in agreement with previous experimental results.[10] It is easy to find that under these circumstances, $S_{analyte}$ is one to two orders of magnitude lower than what is shown in Fig. 4(a) and 4(b). Moreover, because of the fact that quasi-TE mode confines light in the slot whereas the quasi-TM mode enables the majority of light remain in the high-index silicon rib, $S_{analyte}$ appears much larger in Fig. 4(c) and 4(d) than in Fig. 4(e) and 4(f).

$$S_{analyte} = \frac{\partial \lambda_0}{\partial n_{analyte}} = \frac{\partial \lambda_0}{\partial n_{eff}^{TE/TM}} \frac{\partial n_{eff}^{TE/TM}}{\partial n_{analyte}} = \frac{\lambda_0}{n_{eff}^{TE/TM}} \frac{\partial n_{eff}^{TE/TM}}{\partial n_{analyte}} \tag{3}$$

IV. DISCUSSIONS AND CONCLUSIONS

There are generally two kinds of detection schemes for refractive index sensors. One is to detect the power variation with refractive index change. The other is to detect the wavelength shift. The first scheme is simple and easy to be realized and only needs monochromatic wavelength. Of course, this scheme puts a strict demand on the power stability of the optical source. The shape of the spectra is very important for the sensitivity: sharper shape means higher sensitivity. The wavelength-shift-based sensors, such as surface-plasmon-resonance-based sensors, have no requirement on the power stability. But they need extra wavelength-selective devices. The shape of the spectra is very important for the detection limit: sharper shape means lower detection limit. For typical evanescent-field-based sensors, such as ring resonators, the shape of the valley can be very sharp which is good for both of the detection schemes. For our polarimetric interference sensor, the cosine-based transmission spectra is not sharp and so it is not good for the power-variation detection scheme. It is better to be used as a wavelength-shift-based sensor.

Comparing evanescent-field-based non-polarimetric sensors (ring resonators, gratings, *et al.*) and polarimetric interference sensors (such as loop mirror in our paper), the sensing mechanism is totally different. For evanescent-field-based non-polarimetric sensors (ring resonators, gratings, *et al.*), n_{eff} changes with $n_{analyte}$, the sensitivity can be considered as derivative of n_{eff} with respect to $n_{analyte}$.[19] However, for all polarimetric interference sensor, B changes with $n_{analyte}$, the sensitivity can be considered as the derivative of B with respect to $n_{analyte}$. But if we want to compare the sensitivity of a polarimetric interference sensor and a non-polarimetric interference sensor, we have to consider the full sensitivity as shown in Eq. (2) in our article.

Compared with the wavelength-shift ring resonator sensor (212 nm/RIU),[10] our sensor has a much higher sensitivity, but the cosine-shaped spectra limits the detection limit.

In summary, we have proposed a refractive index sensor by marrying a highly-birefringent slot waveguide with a loop mirror structure based on silicon photonics. The scheme shows birefringence as high as 0.8 in air and 0.6 in water. By comparing its sensing properties with conventional principle that only exploits evanescent field, we have concluded that the sensitivity has been enhanced by 1–2 orders of magnitude and reaches 10^3 nm/RIU in both air and water medium. Besides, due to the compact size and its material system, loop-mirror-based slot waveguide sensor could find possible potentials in lab-on-a-chip device or be integrated with other silicon photonic elements.

ACKNOWLEDGMENTS

F. Xu and Y.-q Lu acknowledge the support from National 973 program under contract No. 2011CBA00200 and 2012CB921803, NSFC program No. 11074117 and 60977039, and the Priority Academic Program Development of Jiangsu Higher Education Institutions (PAPD).

[1] Almeida, V. R., Xu, Q. F., Barrios, C. A., and Lipson, M., "Guiding and confining light in void nanostructure," Opt. Lett. **29**, 1209–1211 (2004).
[2] Xu, Q. F., Almeida, V. R., Panepucci, R. R., and Lipson, M., "Experimental demonstration of guiding and confining light in nanometer-size low-refractive-index material," Opt. Lett. **29**, 1626–1628 (2004).
[3] Kou, J.-l., Xu, F., and Lu, Y.-q., "Highly Birefringent Slot-Microfiber," IEEE Photon. Technol. Lett. **23**, 1034–1036 (2011).
[4] Kou, J.-l., Guo, W., Xu, F., and Lu, Y.-q., "Highly Birefringent Optical-Fiberized Slot Waveguide for Miniature Polarimetric Interference Sensors: A Proposal," IEEE Sensors J. **12**, 1681–1685 (2012).
[5] Barrios, C. A., Sanchez, B., Gylfason, K. B., Griol, A., Sohlstrom, H., Holgado, M., and Casquel, R., "Demonstration of slot-waveguide structures on silicon nitride / silicon oxide platform," Opt. Express **15**, 6846–6856 (2007).
[6] Koos, C., Vorreau, P., Vallaitis, T., Dumon, P., Bogaerts, W., Baets, R., Esembeson, B., Biaggio, I., Michinobu, T., Diederich, F., Freude, W., and Leuthold, J., "All-optical high-speed signal processing with silicon-organic hybrid slot waveguides," Nat. Photon. **3**, 216–219 (2009).
[7] Yang, A. H. J., Moore, S. D., Schmidt, B. S., Klug, M., Lipson, M., and Erickson, D., "Optical manipulation of nanoparticles and biomolecules in sub-wavelength slot waveguides," Nature **457**, 71–75 (2009).
[8] Pandey, S., Kumar, G., and Nahata, A., "Slot waveguide-based splitters for broadband terahertz radiation," Opt. Express **18**, 23466–23471 (2010).
[9] Feng, N.-N., Sun, R., Michel, J., and Kimerling, L. C., "Low-loss compact-size slotted waveguide polarization rotator and transformer," Opt. Lett. **32**, 2131–2133 (2007).
[10] Barrios, C. A., Gylfason, K. B., Sanchez, B., Griol, A., Sohlstroem, H., Holgado, M., and Casquel, R., "Slot-waveguide biochemical sensor," Opt. Lett. **32**, 3080–3082 (2007).
[11] Angulo Barrios, C., "Optical Slot-Waveguide Based Biochemical Sensors," Sensors **9**, 4751–4765 (2009).
[12] Dell'Olio, F. and Passaro, V. M. N., "Optical sensing by optimized silicon slot waveguides," Opt. Express **15**, 4977–4993 (2007).
[13] Bettotti, P., Pitanti, A., Rigo, E., De Leonardis, F., Passaro, V. M. N., and Pavesi, L., "Modeling of Slot Waveguide Sensors Based on Polymeric Materials," Sensors **11**, 7327–7340 (2011).
[14] Barrios, C. A., Banuls, M. J., Gonzalez-Pedro, V., Gylfason, K. B., Sanchez, B., Griol, A., Maquieira, A., Sohlstrom, H., Holgado, M., and Casquel, R., "Label-free optical biosensing with slot-waveguides," Opt. Lett. **33**, 708–710 (2008).
[15] Yang, S.-H., Cooper, M. L., Bandaru, P. R., and Mookherjea, S., "Giant birefringence in multi-slotted silicon nanophotonic waveguides," Opt. Express **16**, 8306–8316 (2008).
[16] Kou, J.-l., Wang, Q., Yu, Z.-y., Xu, F., and Lu, Y.-q., "Broadband and highly efficient quadratic interactions in double-slot lithium niobate waveguides through phase matching," Opt. Lett. **36**, 2533–2535 (2011).
[17] Mortimore, D. B., "Fiber loop reflectors," IEEE J. Lightwave Technol. **6**, 1217–1224 (1988).
[18] Passaro, V., Dell'Olio, F., Ciminelli, C., and Armenise, M., "Efficient Chemical Sensing by Coupled Slot SOI Waveguides," Sensors **9**, 1012–1032 (2009).
[19] Passaro, V., Dell'Olio, F., Casamassima, B., and De Leonardis, F., "Guided-Wave Optical Biosensors," Sensors **7**, 508–536 (2007).